We are IntechOpen, the world's leading publisher of Open Access books Built by scientists, for scientists

4,800
Open access books available

122,000
International authors and editors

135M
Downloads

Our authors are among the

154
Countries delivered to

TOP 1%
most cited scientists

12.2%
Contributors from top 500 universities

CLARIVATE ANALYTICS BOOK CITATION INDEX INDEXED

WEB OF SCIENCE™

Selection of our books indexed in the Book Citation Index in Web of Science™ Core Collection (BKCI)

Interested in publishing with us?
Contact book.department@intechopen.com

Numbers displayed above are based on latest data collected.
For more information visit www.intechopen.com

8

In-line Typed High-Precision Polarization Lidar for Disaster Prevention

Tatsuo Shiina
Graduate school of Advanced Integration Science,
Chiba University
Japan

1. Introduction

Prediction of local and steep weather change such as heavy rain and lightning strike are urgently needed for disaster prevention. In Japan, Automated Meteorological Data Acquisition System (AMeDAS) has been operational throughout the country, with a mesh size of 20 km. Lightning Location Positioning (LLP) system, Lightning Position and Tracking System (LPATS), and SAFIR (Surveillance et Alerte Foudre par Interférometrie Radioélectrique) have been also used for lightning detection. (MacGorman & Taylor, 1989; Théry, 2001; Hayashi, 2006; Matsudo et al, 2007; Hauf et al, 2007) All of these weather observation systems, however, are comprehensive and necessary to analyze the multipoint data for the weather forecast in a certain area.

Heavy rain and lightning strike locally occur during a short time period. They are often broken out at low-altitude and mainly caused by ice-crystals in cloud. Such local and steep weather change should be observed and be distinguished at a point observation. Radar (Radio Detection and Ranging) is a solution to catch weather change, but it can only detect rain droplets and cannot detect cloud particles which are precursors of heavy rain. To predict the heavy rain and lightning strike, low-altitude atmosphere and cloud should be observed. Furthermore, the flow of ice-crystals should be monitored.

Lidar (LIght Detection And Ranging) can observe the atmosphere and cloud. It is stand-alone system and can distinguish ice-crystals from water droplets. On the other hand, Lidar technique is unsuited for observation in the near range because the laser beam will be dangerous for human eye.

To develop the disaster prediction system for local weather change, we apply the lidar technique. The system was designed with emphasis on the following characteristics:

Stand-alone
Compactness
Eye-safety

To realize such a system, in-line optics, or common optics for transmitter optics and receiver optics, was adopted. It is usual technique for microscope optics, while the pulsed energy on lidar is too high that no one could accomplish its development since the first proposal. (Measures, 1984) Micro Pulse Lidar (MPL) broke though the problem and built up the new generation in lidar field. (Spinhirne, 1993, 1994 & 2001; Grund & Sandberg, 1996; Lee et al,

Source: Advances in Solid-State Lasers: Development and Applications, Book edited by: Mikhail Grishin,
ISBN 978-953-7619-80-0, pp. 630, February 2010, INTECH, Croatia, downloaded from SCIYO.COM

1996; Welton, 2001; Hwang et al, 2002) Our first developed lidar is also MPL. By installing the in-line optics, near range detection and narrow Field Of View (FOV) observation were realized simultaneously.
After the success of our in-line MPL, the next approach for in-line lidar for high precision polarization measurement was conducted. While it is not eye-safe, it is capable of near range detection and narrow FOV observation.
Though the development of the unique lidars, we brushed up our skill and built up the stand-alone local weather prediction system for disaster prevention.
This chapter introduces the lidar theory, in-line optics, initial and next approach of the original lidar development for low-altitude atmosphere and cloud.

2. Outlook

The goal of our research is the prediction of local weather for prevention of disasters such as heavy rain and lightning strikes. To achieve this, monitoring of the flow of ice-crystals in the cloud is effective. Local and steep weather changes such as heavy rain and lightning strikes occur in the low altitude atmosphere. At first our group developed a compact in-line type micro pulse lidar (MPL) system which can detect local and fast changes in low-altitude clouds and monitor the flow of ice-crystals in clouds by measuring the depolarization effect. (Shiina, 2002, 2005a, & 2005b) Thanks to the in-line optics, the system can detect near range echoes with the narrow field of view of 0.1 mrad. It can also distinguish the ice-crystals from sphere particles by examining the depolarization. The laser pulse energy is in the order of micro joule, and the system is eye-safe. We have succeeded in the prediction of heavy rain, while the prediction of lightning strikes is yet to be accomplished, because the correlation between the ice crystal flow and lightning discharge is indirect. In order to establish direct correlation between the lightning discharge and the transmitted lidar beam, we considered the use of the Faraday effect, by which the electromagnetic pulse due to the lightning discharge rotates the polarization plane of the propagating beam in the ionized atmosphere. By measuring the rotation angle of the polarization plane of the propagating beam, the electron density, discharge current and the lightning position can be estimated. We aim to develop the new concept lidar for lightning discharge detection.
Numerical analysis using a cloud-to-ground discharge model showed that the rotation angle for visible light is <1 degree. (Shiina, 2008a) A laboratory experiment using an impulse voltage generator and a discharge chamber (with a gap length in the order of cm) was conducted, and the experimental results were in agreement with the analysis results. (Shiina, in press) Another laboratory experiment using a larger impulse voltage generator (with a gap length in the order of m) was conducted, and the rotation of the polarization plane of the beam propagating through the immediate vicinity of the discharge path was confirmed. (Shiina, 2008b; Fukuchi, in press)
In order to detect a small rotation angle of the polarization plane, we developed a new concept lidar system for high precision polarization measurement. The isolation between the orthogonal polarizations must be improved up to >30 dB, which was realized by a specially designed polarization- independent optical circulator composed of Glan laser prisms and highly transparent Faraday rotators. Thanks to the in-line optics, the echoes could be detected from near range. We examined the echoes in the viewpoint of accuracy of estimation of rotation angle of the polarization plane and system stability. (Shiina, 2007a)

3. First approach – lidar theory and depolarization measurement -

3.1 Three types of lidar optics

There are three types of fundamental structures of lidar optics.(Shiina, 2005b) A biaxial type shown in Fig.3-1(a) has separate optics for the optical transmitter and the optical echo receiver, and the laser beam is transmitted parallel to the receiver axis. A coaxial type shown in Fig.3-1(b) transmits the laser beam along the receiver axis. An in-line type shown in Fig.3-1(c) has a common optics for the transmitter and the receiver, i.e. the telescope is used for both transmission and reception.

The biaxial and coaxial types have the demerit of having a blind area (non-detectable range of lidar echo) at near range. For the biaxial type, an easy way to shorten the blind area is to broaden the receiver's field of view (FOV), but this increases the background noise and decrease the dynamic range of lidar echo. Another method is to set the path of the transmitted laser beam at a slant angle against the receiver axis. However, in this configuration, the laser beam deviates from the receiver's FOV beyond a certain distance.

In the coaxial type, the laser path and the receiver axis are collinear. This necessitates the implementation of a transmitter mirror (usually located on the back side of the secondary mirror). Therefore, the shadow of the transmitter mirror (secondary mirror) creates a blind area at near range. Furthermore, a pinhole (spatial filter) is usually inserted at the focal point of the receiver telescope in order to narrow the receiver's FOV to eliminate the background light. The lidar echo from near range is out of focus and is blocked by the pinhole, resulting in the blind area.

In contrast, by using in-line typed optics, the laser path is always overlapped with the receiver's FOV even if it is narrow of the order of 0.1 mrad. As the beam size of the transmitted laser beam can enlarged up to the telescope aperture, there is no blind area of near range lidar echoes. There exists the technical problem of separating the transmitted beam and the lidar echoes.

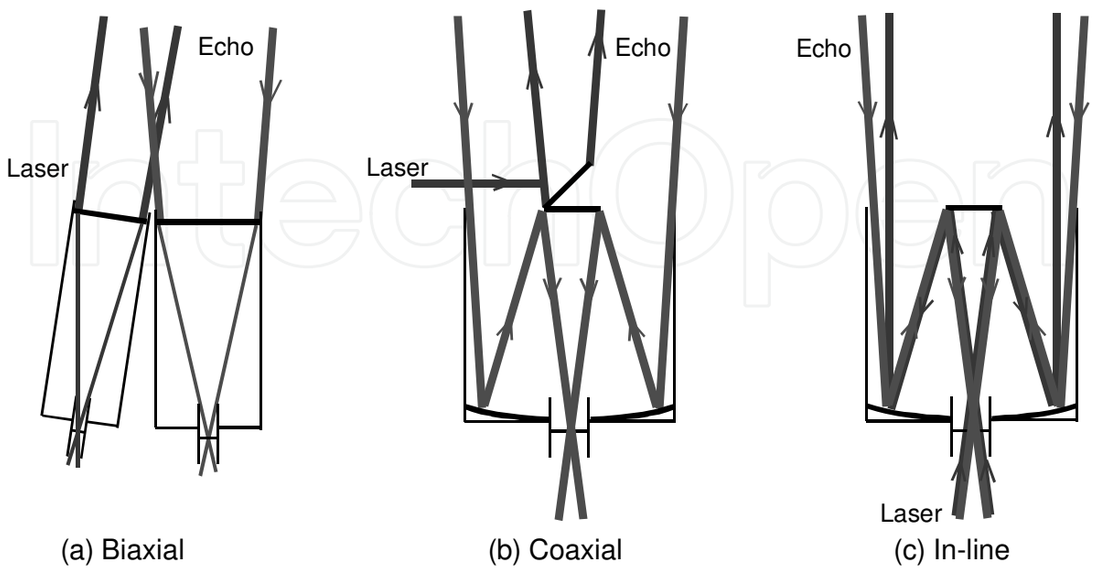

Fig. 3-1. Three types of lidar optics.

3.2 Lidar equation

The lidar echo characteristics were evaluated by calculating the lidar echo power *Pr(L)* and its signal-to-noise ratio *SNR(L)*.(Measures, 1984; Weitkamp, 2005; Fujii & Fukuchi, 2005)

$$Pr(L) = P_0 K A_r \frac{c\tau}{2} \beta(L) Y(L) T(L)^2 / L^2 + Pb$$
$$T(L) = \exp(-\int_0^L \alpha(l) dl) \tag{3-1}$$

$$SNR(L) = \frac{\sqrt{M}\sqrt{\eta \Delta t / h\nu}\,\Pr(L)}{\sqrt{\mu}\sqrt{\Pr(L) + Pd}} \tag{3-2}$$

where, P_0 is the transmitting power, K is the system optical efficiency, A_r is the receiver's area, c is the speed of light, τ is the pulse width, $\beta(L)$ is the backscattering cross section, $Y(L)$ is the geometrical form factor, $T(L)$ is the transmittance, Pb is the background light power, $\alpha(L)$ is the atmospheric extinction coefficient, M is the number of signal summation, η is the detector's quantum efficiency, μ is the detector's noise factor, h is Planck's constant, υ is the light frequency, Pd is the equivalent dark current power.

The collimated beam is transmitted to the atmosphere, scattered in all directions, and a small part of the scattered light is collected by the receiver. The fraction of the scattered light returning to the receiver is proportional to the solid angle subtended by the receiver aperture, so the lidar echo intensity is inversely proportional to the square of the distance (from the location of the lidar to the point at which the scattering occurs). The transmitted beam and the backscattered echo are attenuated by the atmospheric transmittance, i.e., due to the atmospheric extinction coefficient. The geometrical form factor *Y(L)* is an overlap function between the receiver's FOV and the transmitting beam. It is determined by the specifications of the transmitted laser beam, the receiving telescope, and the field stop aperture. (Halldorsson & J. Langerholc, 1978; Harms, 1979; Sugimoto et al, 1990)

3.3 Simulation

The lidar echo was estimated for the three type lidars: the coaxial type lidar, the improved coaxial type lidar, and the in-line type lidar with an annular beam. The specifications are summarized in Shiina, 2005b. The coaxial type and the improved type lidars have been put to practical use. The transmitting beam was fired from the center of the telescope, generally on the secondary mirror. The improved coaxial lidar was designed for near range echo measurement. The divergence of the transmitting beam and the receiver's FOV were larger than those of the coaxial type lidar. A photomultiplier (PMT) was used as the detector in the case of the improved coaxial type lidar, while and avalanche photodiode (APD) was used for other lidar types. The coaxial type lidar is the typical compact lidar. The intensity of the transmitting beam was nearly equal in these models, while their intensity distributions and aperture sizes were different.

At first, the geometrical form factor *Y(L)* was examined. The result is shown in Fig. 3-2(a). The *Y(L)* of the improved coaxial type lidar has the fastest rise of the three. This is because the beam divergence and the receiver's FOV were large. The *Y(L)* of the in-line type lidar rises slowly and needs a longer distance to reach unity. The important point, however, is the receiver's efficiency at near distance for the lidar echo estimation. The coaxial type lidar cannot detect the echo within 0.2 km in this condition. The *Y(L)* of the in-line type lidar

never becomes 0 and is higher than that of the other two type lidars at the nearest distance. This effect is due to the similarity between the intensity distribution of the annular beam and the receiver's efficiency distribution in the near range. The lidar echo variations along the propagated distance are shown in Fig. 3.2(b). The atmospheric extinction coefficient was α=1.70x10^{-4}/m and the backscattering coefficient was β=3.4x10^{-6}/m. The usual lidar echo variation along the propagated distance has a peak such as that of the coaxial type and the improved coaxial type lidar. The peak is caused by the relation between the geometrical form factor *Y(L)* and the lidar echo intensity *P(L)*, which both depend on the propagated distance. On the other hand, the echo variation of the in-line type lidar has no peak, i.e., the lidar echo is maximum at the nearest distance and decreases monotonously along the propagated distance. This is mainly due to the efficiency of the geometrical form factor in the near range. Although the improved coaxial type lidar had the high signal-to-noise ratio in the near range, the ratio decreases rapidly along the further propagated distance in comparison with those of the coaxial and the in-line type lidar. The improved coaxial type lidar needs the distance of more than a few kilometers to obtain the ideal echo variation, in which the lidar echo is inversely proportional to the square of the propagated distance. The in-line type lidar approximately has the ideal echo variation from the nearest distance. This facilitates the analysis of the near range echo, because there is no need for compensation for the variation of the factor *Y(L)*. The result also indicates that the in-line type lidar can detect any obstructions (human, building, etc.) without blind range.

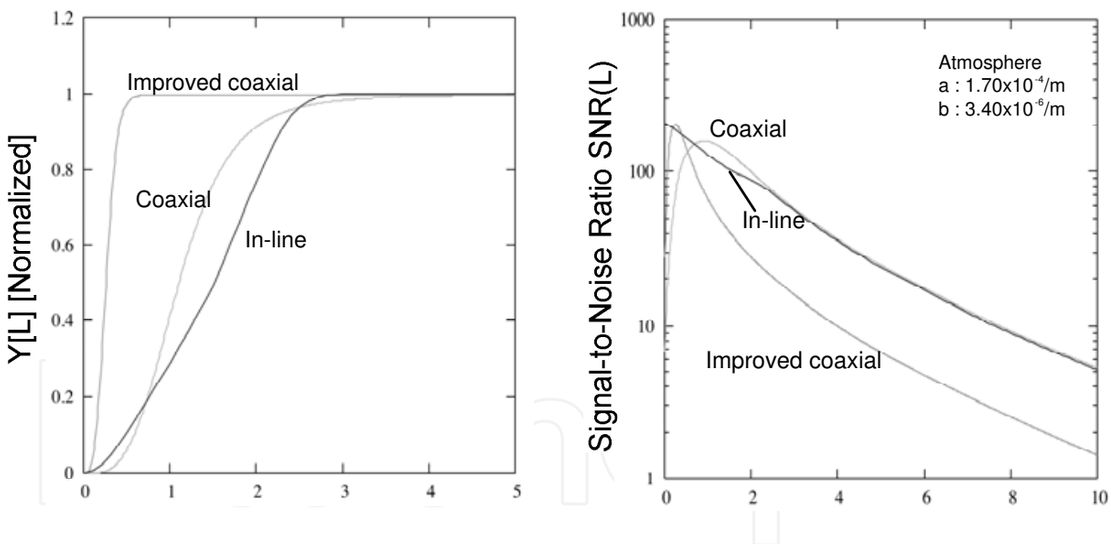

Fig. 3-2. Geometric form factor Y(L) and Signal-to-Noise ratio SNR(L) with the three lidars.

3.4 Depolarization measurement

Small particles suspended in the atmosphere include aerosols, raindrops, cloud particles, ice-crystals. Rayleigh scattering and Mie scattering are commonly used for lidar observation. Cloud particles, which we intend to measure, have a diameter of about 5 μm, and cause Mie scattering. (Pal & Carswell, 1973; Ryan et al, 1979; Sassen, 1991; Zaccanti et al, 1993; Gai et al, 1996) The polarization plane of incident bream and backscattering echo against a cloud

particle and an ice-crystal are illustrated in Fig. 3-3. In the scattering, the backscattering echoes keep the incident polarization plane when the beam hits the cloud particles (spherical particles). On the contrary, non-spherical particles such as ice-crystals change the incident polarization. It is known as depolarization effect. It is caused by the difference of Fresnel's refraction coefficient between the parallel and the orthogonal polarization. When the beam hits the plane surface of ice-crystal perpendicularly, the depolarization never occurs. When the beam hits the crystal at an angle, one can distinguish the ice-crystals from the spherical particles such as cloud particles by examining the orthogonal polarization components of the lidar echoes.

The spherical particles, however, cause depolarization in the case of multiple scattering. (Sassen & Petrilla, 1986; Kerscher, 1995; Bruscaglioni et al, 1995) To reduce the contribution of multiple scattering, it is effective to narrow the receiver's FOV. The biaxial and coaxial lidars with narrow FOV have a broad blind area, because it a certain distance is needed for the transmitted beam to enter into the receiver's FOV (the overlap function has a slow rise with respect to distance). In contrast, the in-line type lidar can have a narrow FOV with no blind area.

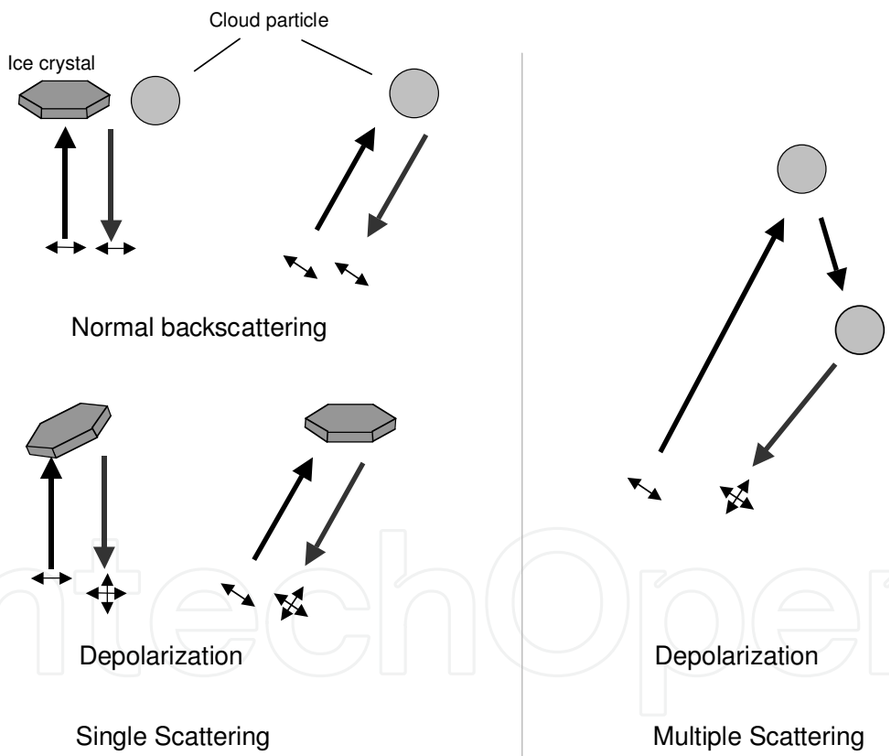

Fig. 3-3. Normal backscattering and depolarization by ice-crystals and cloud particles.

4. First Approach – In-line MPL-

4.1 Apparatus

The setup of the in-line MPL is illustrated in Fig. 4-1. The optical circulator and the pair of Axicon prisms were installed into the lidar optics. (Shiina, 2005a) The laser source is a LD pumped YLF laser, of wavelength 1.047μm, pulse width 5 ns, output energy 80μJ, and

maximum pulse repetition frequency 50 kHz. The transmitted beam is collimated by the beam expander just behind the laser head and passes though the optical circulator.
The optical circulator makes allows measurement of the orthogonally polarized echoes with two detectors, that is, the same polarized component (p-component) as the transmitting beam and the orthogonal one(s-component).(Shiina, 2002) The s-component echo is reflected at the polarized beam splitter (PBS2) and goes to the detector APD(s), while the p-component echo passes through the circulator optics and goes to the detector APD(p) (See Fig.4-2). The insertion and isolation characteristics of the optical circulator are summarized in Table 4-1. The insertion loss as the transmitter is 2dB and the isolation between the orthogonal polarized echoes is about 20dB. As the insertion loss of the Faraday rotator was large, the sensitivity of the s-component echo became twice of that of the p-component one. It is convenient to estimate the depolarization effect by comparing the weak s-component echo with the p-component one. All optical elements have small tilts (1.5 degrees) against the optical axis. The laser head also has a tilt of 3 degrees against the optical axis. As the in-line MPL could not reject the directly reflected light from the lidar optics perfectly, the reflected light influenced the lidar echo signal (ringing or saturation of the lidar receiver's electrical circuit, etc.). Pinholes were inserted in front of the detectors (APDs) in order to prevent the light directly reflected from the in-line optics from entering the detectors. Its aperture was determined in combination with the tilts of the in-line optics.
In the in-line type lidar, the same telescope is used for transmission and reception. When the transmitted beam passes through the telescope, part of the beam is reflected by the secondary mirror, obstructing the transmitted beam and causing a large noise signal upon returning to the detector. Therefore, a pair of Axicon prisms was installed to prevent this reflection. The prism pair creates an annular beam, whose hole overlaps the secondary mirror of the reflecting telescope. The insertion loss of the transducer was 0.932 dB. The insertion loss of the whole lidar optics was about 3 dB. The total energy of the output beam was 8 kW. The eyepiece focuses the transmitting annular beam at the field stop aperture (FSA). The FSA is a pinhole of 650 μm diameter. At the focal point, the annular beam changes its beam shape into the nearly non-diffractive beam, of which spot size is less than 4μm diameter . (Belanger & Rioux, 1978; Durnin & Miceli, 1987; Indebetouw, 1989; Scott & McArdle, 1992; Arrimoto et al, 1992; Doskolovich et al, 1993; Kono, 1995 & 1996; Soifer et al, 1997) The beam then passes though the FSA without any obstruction. The annular beam finally goes to the telescope. A Schmidt-Cassegrain reflecting telescope was used for the transmitter and receiver. The annular beam was expanded up to the telescope aperture (304 mm diameter). The quality of the transmitting beam was verified by the identification between the annular beam enlarged by the telescope and that in front of the eyepiece. The light directly reflected from the in-line optics was suppressed to below 0.1 mW. The FOV of the telescope is 0.1 mrad, determined by the focal length of the telescope and the aperture size of the FSA. The divergence of the transmitting beam can be controlled by the beam expander. Though the divergence does not depend on the telescope's FOV, it is basically less than the FOV.
The detectors are NIR enhanced Si-APDs (PerkinElmer 30954E). They have responsivity of 36 A/W at wavelength 1064 nm and at the operating voltage. The responsivity rises up over 500 A/W near the breakdown voltage. The voltage over the breakdown is in the region of the Geiger mode. In our system, the APDs were used in the analog mode between the operating voltage and the near breakdown voltage. All optics including the laser head and the detectors were mounted on the telescope tube. It allows measurement of lidar echoes

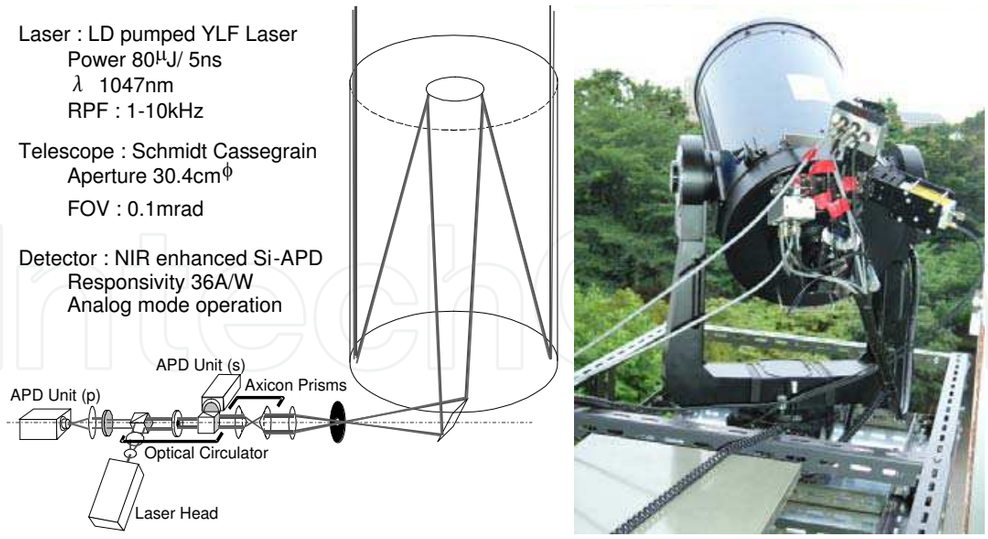

Fig. 4-1. Optics of In-line typed micro pulse lidar.

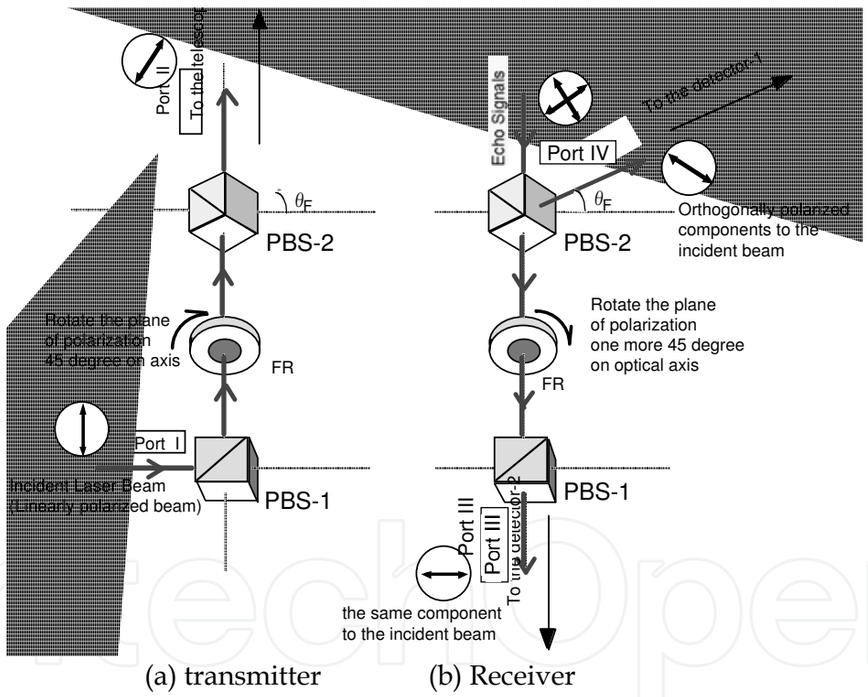

Fig. 4-2. The optical circulator for in-line type lidar.

	Port I	Port II	Port III	Port IV
Transmitter	- (Incident TEM00 Mode)	2.08	>60.0	>60.0
Receiver	-	- (Parallel component to the incident beam)	3.27	21.5
	-	- (Normal component to the incident beam)	17.2	0.50

Table 4-1. Insertion and isolation characteristics of the Optical Circulator in Decibels.

from the near distance with the narrow FOV. The incident beam energy into an human eye was 5.34 J/s. It is lower than the maximum permissible exposure (MPE) value of 11.4 J/s in the same condition. (American National Standards Institute, 1986) The in-line MPL keeps eye-safety even in front of the system.

4.2 Near range observation

Figure 4-3 shows the observation results of ice-clouds during 22:40-4:20 local time (JST) on January 24, 2009. Lidar echoes of p- and s- components were captured simultaneously. The observation angle was 4 degrees from zenith. In General, ice-crystals in the sky are parallel to the ground.(Sassen, 1991) Since the angle of incidence was too small, echoes observed from upper clouds at the altitude of 1200-2000 m (A) (B) contained only p-component, while sparse and intensive s-component echoes were widely captured from cloud at the altitude of 600-1800 m (C) during 22:40-3:00. Especially strong echo was detected in s-component echo during 2:40-3:00 (D). In this period, strong wind was also observed in that period. Since ice-crystals leaned against the zenith direction while falling, ice-crystal echoes were captured in s-component.

The downdraft could be also recognized by lowering of the cloud base. Although snowfall or downfall could not be observed on the ground, the ice-crystals would have melted away during descent because the ground temperature was about 4 degrees.(Sassen, 1991) Indeed, both of the p- and s-component echoes could not been detected near the ground. The in-line typed MPL with the narrow FOV and depolarization measurement can examine dynamics of ice-crystals in low-altitude clouds.

Next, measurement of heavy rain and thundercloud are shown in Fig.4-4. The eve of the heavy rain was observed in the low altitude atmosphere at July 4, 2006, as shown in Fig.4-4(a). The cloud base was around 1200 m and above. At 17:00, strong echoes (p-component) appeared at very low altitude (100-600 m). The echoes reached near ground, while it did not grow up to the cloud base. The downfall was not detected on the ground. Although the droplets caused the strong echoes could not distinguished by visual contacts, heavy rain started just after the observation. The system could detected the steep change in low-altitude and local area. Low altitude thundercloud was also observed as a trial at the evening on July 14, 2006, as shown in Fig.4-4(b). The cloud base came close to the ground; about 400 m. Strong echoes appeared in the cloud. The cloud echoes usually come from the cloud base, and decrease exponentially over a characteristic distance of about 300 m. The result of thundercloud did not show such a exponential change, but showed strong signals in the cloud. It is not easy to clear the casual correlation between the thundercloud echoes and thunder activity. To capture the precursors of the lightning and predict the lightning strike, we must catch more direct sign from the lightning.

5. Next step – Direct detection of lightning discharge-

5.1 Faraday effect

The interaction between the light and the atmosphere is caused by scattering (Mie, Rayleigh, Raman), and also by the magneto-optical effect and electro-optical effect. The magneto-optical effect (Faraday effect) is associated with the lightning discharge. It has been reported as an optical measurement method for magnetic confinement fusion reactor. (Kawahata & Okajima, 2000) The polarization plane of a beam propagating parallel to the magnetic flux is rotated in a partially ionized atmosphere (plasma) (Fig.5-1). The rotation angle is

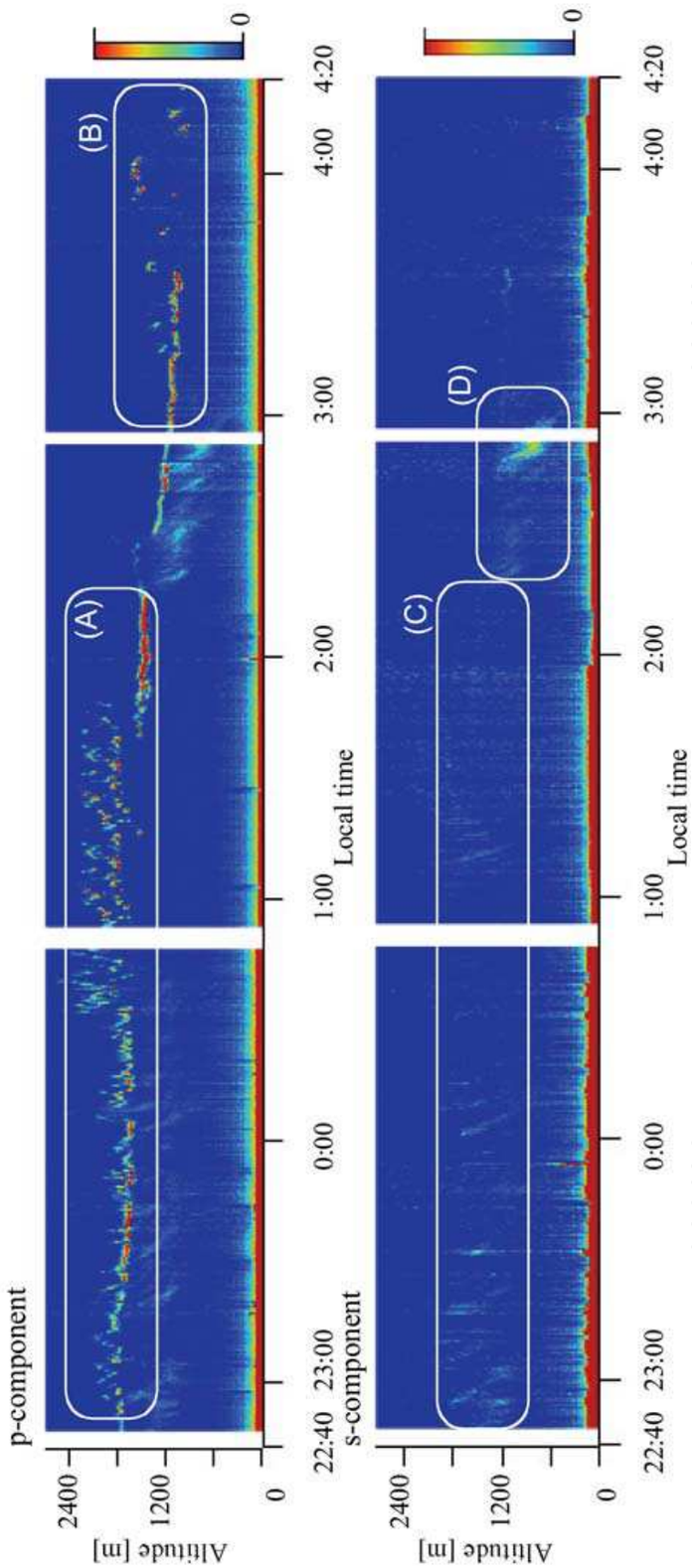

Fig. 4-3. long term ice-cloud measurement. January 24, 2009. Temp. 3.7deg Hum. 70% Cloudy

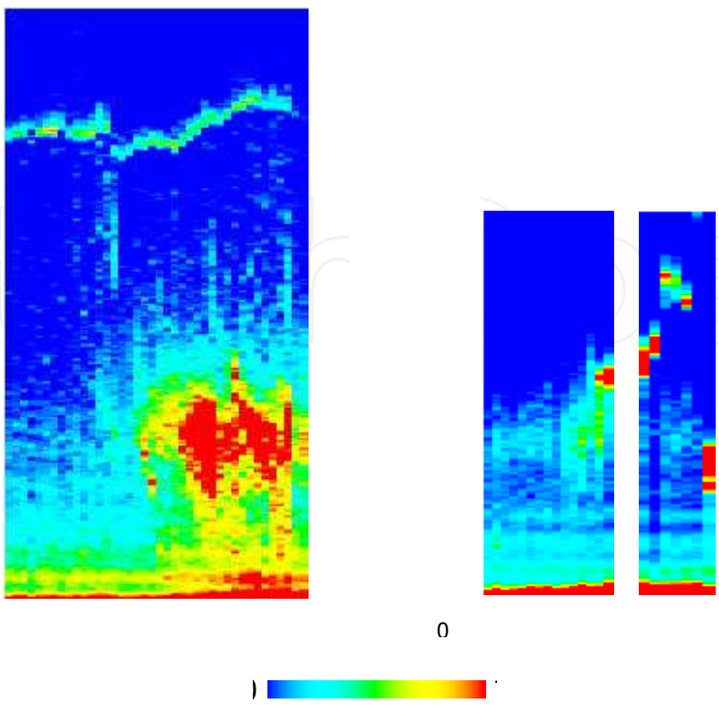

Fig. 4-4. lidar echoes (p-components) in bad weather condition. (a) July 4, 2006. Temp. 28deg. Hum. 52%. Before heavy rain (b) July 14, 2006, Temp. 32deg. Hum. 50% Thunder cloud

proportional to the product of the ionization electron density n_e and the magnetic flux density B along the beam propagation path. The linearly polarized beam can be regarded as a combination of the clockwise and the counterclockwise circularly polarized beams. The refractive indices of the ionized atmosphere for each circularly polarized beam are as follows.

$$n_{\pm} = \left(1 - \frac{\omega_{pe}^2}{\omega^2}\frac{\omega}{\omega \pm \omega_{ce}}\right)^{1/2}$$
$$\omega_{pe} = \sqrt{\frac{e^2 n_e}{\varepsilon_0 m_e}} \quad \omega_{ce} = \frac{eB}{m_e} \tag{5-1}$$

where ω_{pe}, ω_{ce} are the plasma and electron cyclotron frequencies, respectively, e is the fundamental charge, m_e is the electron mass, and ε_0 is the permittivity of free space. Therefore, the rotation angle of polarization of the beam propagated at distance L (=L_1~L_2) is obtained as follows.

$$\begin{aligned}\delta &= \frac{\pi}{\lambda}\int_{L_1}^{L_2}(n_+ - n_-)dl \\ &= 2.62\times 10^{-13}\lambda^2\int_{L_1}^{L_2} n_e B dl\end{aligned} \tag{5-2}$$

where λ is wavelength of the propagating beam. Since δ is proportional to λ^2, the rotation angle for visible light is small. Therefore, the polarization angle rotation must be measured with high accuracy in order to detect lightning discharge.

When the Faraday effect is applied to lightning measurement, the atmosphere needs to be partially ionized, and the magnetic flux due to the lightning discharge must exist. Cloud-to-cloud discharge, which causes 20-30 times continuous discharge, satisfies those conditions. (Franzblau & Popp, 1989; Franzblau, 1991; Stith et al, 1999; Society of Atmospheric Electricity of Japan, 2003)

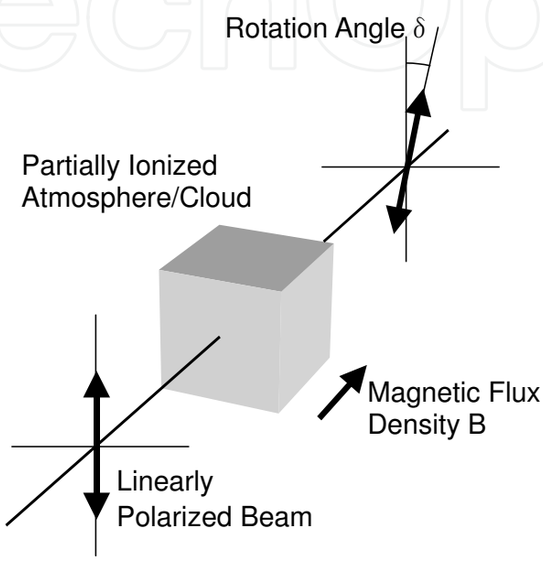

Fig. 5-1. Faraday effect.

5.2 New concept lidar

The analysis and experimental results have shown that the rotation angle of polarization plane of the propagating beam is less than 1 degree, so that the mutually perpendicular polarization components must be measured with a sensitivity and accuracy of >30 dB in order to detect lightning discharges. The rotation of the polarization plane only occurs in a nearly perfectly ionized atmosphere, so the signal cannot be detected unless the transmitted beam intersects the discharge path. On the other hand, the shock wave (variation in the neutral gas density) generated by the discharge can be detected over a broader range, while it causes no rotation of the polarization plane. (Fukuchi, 2005) This was confirmed by high voltage discharge experiment in the next section.

Therefore, the scenario of the lightning detection using the lidar system is designed as follows. At first the system roughly scans the sky in the direction in which the occurrence of a cloud-to-cloud lightning discharge is likely. If a shock wave is detected, the 3-demensional lightning position is estimated. Next, by scanning the neighborhood of the lightning position with higher precision to intersect the propagating beam and the lightning discharge path, the rotation angle of the polarization plane is measured. In general, lower area (bottom) of clouds will be scanned, as the beam penetrates only a few hundred meters in clouds. The distribution of the discharge location and its change will lead to the prediction of lightning strike.

The lidar system must be capable of measurement at near range with a narrow field of view in order to eliminate the effects of multiple scattering. The use of in-line optics is effective in meeting this requirement. The system must also have scanning capability to search the cloud-to-cloud lightning discharge. The concept of the lidar system for lightning detection is shown in Fig.5-2. For the detection of the small rotation angle, differential detection should be used.

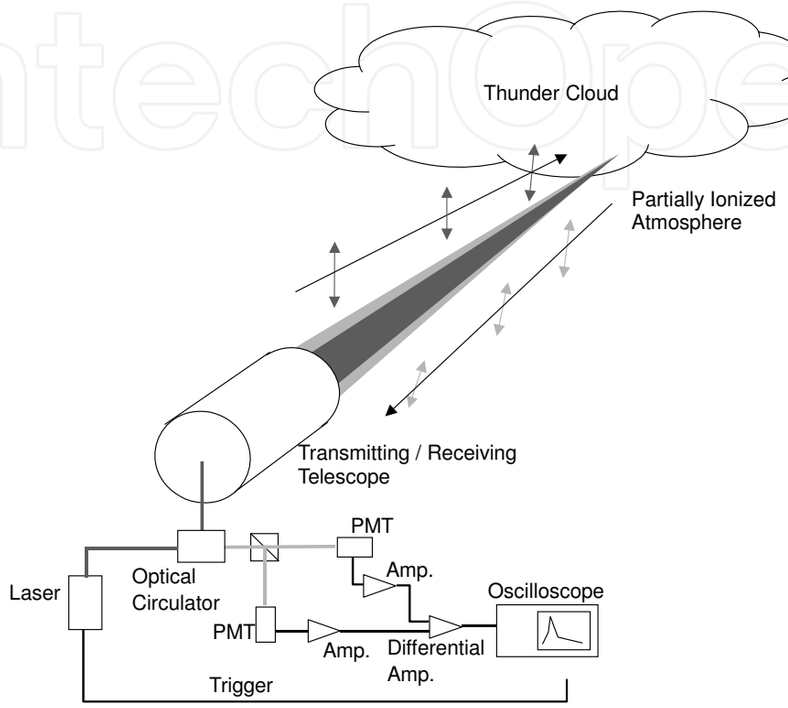

Fig. 5-2. Concept of lidar lightning detection.

6. Demonstration –Ground based experiment-

6.1 Apparatus

Figure 6-1 shows the experimental setup of the high-voltage discharge experiment. (Shiina, 2008b; Fukuchi, in press) The experiment was conducted in a high voltage experiment hall using an impulse voltage generator (HAEFELY SGΔA1600-80). The discharge gap between the needle electrodes was 0-2 m and the charging voltage was >1000 kV. A voltage divider and Rogowski coil were used to measure the charge voltage and the discharge current. The laser beam was transmitted near the discharge path. The polarization plane of the linearly polarized laser beam was so adjusted by a half wave plate (HWP) that its photon flux was equally divided into the two mutually orthogonal polarization components. The intensities of the orthogonal polarization components were detected by photodiodes (PDs) with amplifiers. A differential amplifier was also installed in the receiver circuit to detect the small rotation angle of the polarization plane. To eliminate electromagnetic noise caused by the discharge, the laser power supply and the receiver circuit were placed inside copper boxes. Signal cables were also shielded by wire mesh. The specifications of the discharge equipment and the optical detection system are summarized in Table 6-1. The differential output was detected only when the polarization plane was rotated by the Faraday effect.

The position of the propagating beam could be adjusted with respect to the discharge path and the discharge terminals.
The rotation angle of the polarization plane was estimated from the intensities of the orthogonal polarization components or the differential output by eq.(6-1). I_p and I_s are the intensities of the orthogonal polarization components.

$$\delta = \frac{\pi}{4} - \tan^{-1}(\sqrt{I_s} / \sqrt{I_p}) = \tan^{-1}(\frac{\sqrt{I_p} - \sqrt{I_S}}{\sqrt{I_P} + \sqrt{I_S}}) \quad (6\text{-}1)$$

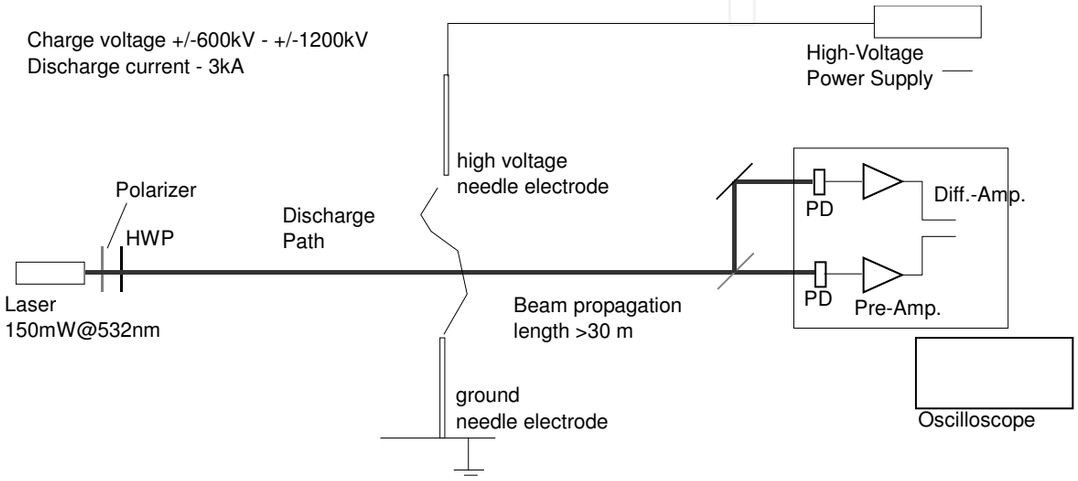

Fig. 6-1. Experimental setup of the high voltage discharge experiment.

When $|Ip\text{-}Is| << Ip, Is$, the rotation angle is approximated by the following equation.

$$\delta = \frac{I_p - I_s}{I_p + I_s} \quad (6\text{-}2)$$

The estimation of the rotation angle is illustrated in Fig. 6-2. The polarity of the rotation angle indicates the spatial relation between the beam and the discharge path.

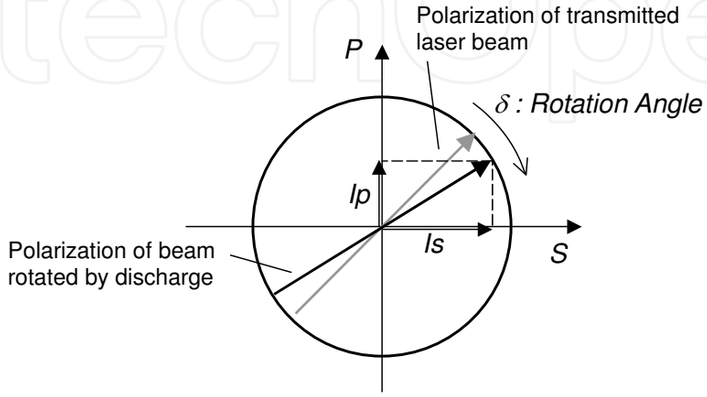

Fig. 6-2. Differential detection.

Discharge equipment	
Manufacturer, model	HAEFELY SG ΔA1600-80
Maximum charging voltage	+/-1600 kV
Discharge waveform	Lightning Impulse
Electrodes	needles
Discharge gap length	0-2 m
Beam/Receiver	
Light source	Nd:YAG green laser λ=532 nm, CW
Power	150 mW
Detector	Photodiode + Amplifier
detection	Differential detection

Table 6-1. Specifications of the discharge equipment and the optical detection system

6.2 Rotation angle detection

6.2.1 Detection of shock waves

Lightning discharge generates shock waves, which accompany variations in the air density and cause fluctuations of the propagating beam.(Fukuchi, 2005) Signals due to the shock waves are shown in Fig. 6-3. The discharge gap between the needle terminals was 77 cm and the charge voltage was –1200 kV. The propagating beam passed 4 cm below and 3 cm to the left of the high voltage needle electrode. In this case, the rotation angle was not detected because of the spatial separation between the discharge path and the beam. The air density variation accompanying the shock wave does not contribute to the Faraday effect, so the differential output is zero. In Fig. 6-3, the shock wave appeared 30 μs after the discharge trigger, so the distance between the discharge path and the propagating beam was calculated as 1 cm. In the experiment, we confirmed that the shock wave could be detected at a few hundred μs after the discharge trigger. Therefore, the shock wave signal can be used an indicator to locate the discharge location.

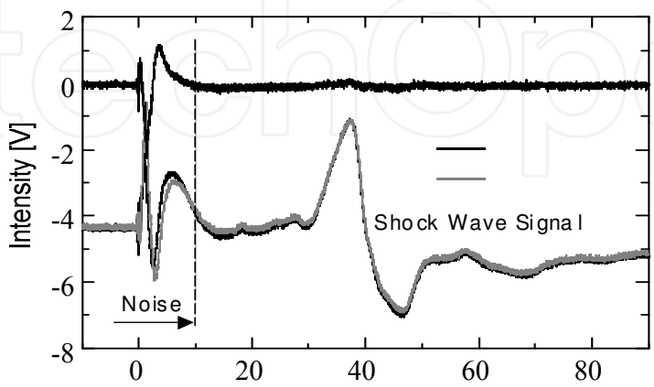

Fig. 6-3. Detection of shock wave.

6.2.2 Detection of polarization rotation angle

The differential output signals corresponding to the rotation angle of the polarization plane are shown in Fig.6-4. The typical discharge current is also shown. The discharge gap between the needle terminals was 77 cm and the charging voltage was +/–1200 kV. The propagating beam passed 2 cm under the high voltage needle electrode. The waveform before 10 μs could not be evaluated because of the electromagnetic noise due to the discharge. The differential outputs in the case of positive discharge (+1200 kV) and negative discharge (-1200 kV) showed opposite polarity. The output signals had the same response time as the discharge current. The rotation angle evaluated using eq. (6-1) was δ=0.53 degrees for positive polarity and δ=0.50 degrees for negative polarity. The dynamic range of >30 dB of the differential amplifier enabled detection of the small rotation angle. The results were in agreement with the results of numerical analysis and preliminary experiment using short gap discharge.

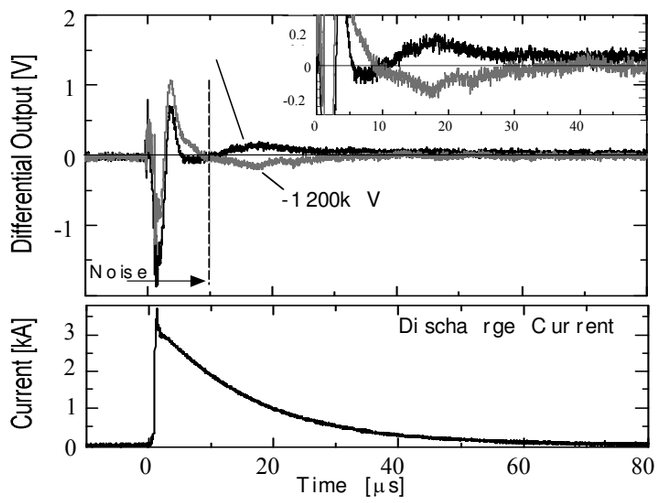

Fig. 6-4. Obtained waveform showing rotation angle detection for positive and negative polarities.

To suppress the electromagnetic noise, the receiver optics and electrical circuits were put in a shielded room. Due to spatial limitations caused by the introduction of the shield room, the position of the propagating beam was changed to 30 cm above the ground needle electrode from 2cm below the high voltage needle electrode. The electron density does not change significantly in the discharge path on arc or spark discharge. The discharge gap length was extended from 77 cm to 100 cm. This caused the shot-to-shot fluctuations of the discharge path in the extended discharge gap. The rotation angle depends on the distance between the discharge path and the propagating beam. Figure 6-5 shows the results of the experiment. The discharge gap between the needle terminals was 100 cm and the charge voltages were +1200 kV. Fig. 6-5(a) shows the differential output signals. The influence of the electromagnetic noise on the waveform decreased in comparison with the former experiment. Photographs of the discharge path in Fig. 6-5(b) were obtained simultaneously with the waveforms in Fig. 6-5(a). The position of the propagating laser beam is also indicated. The separation distance between the beam center and the discharge path was <2

cm for (A) and >6 cm for (B). The rotation angle was estimated as 0.54 degrees in case (A). The existence of the differential output is dependent on the distance between the discharge path and the beam. The output signal thus appeared when the probing beam was located within 2 cm apart from the discharge path, where the atmosphere was nearly perfectly ionized (n_e~10^{25} m^{-3}).

The present sensitivity of the rotation angle of the polarization plane is <1 degree. It is sufficient to detect the rotation angle only in a perfectly ionized atmosphere (n_e~10^{25} m^{-3}). The rotation angle can be detected only if the transmitting beam crosses the neighborhood of the discharge path. On the other hand, the shock wave does not rotate the polarization plane, and can be detected over a broader spatial region. Therefore, the observation algorithm for lidar application is designed as follows. At first, the lidar system roughly scans the observation region. When a shock wave is detected, the lightning position is estimated. Next, the neighborhood of the lightning position is scanned with higher spatial resolution, and the rotation angle of the polarization plane is measured. The discharge current, magnetic flux density, and ionized density of atmosphere are estimated. The distribution of the ionized atmosphere and its change will lead to the prediction of lightning strike.

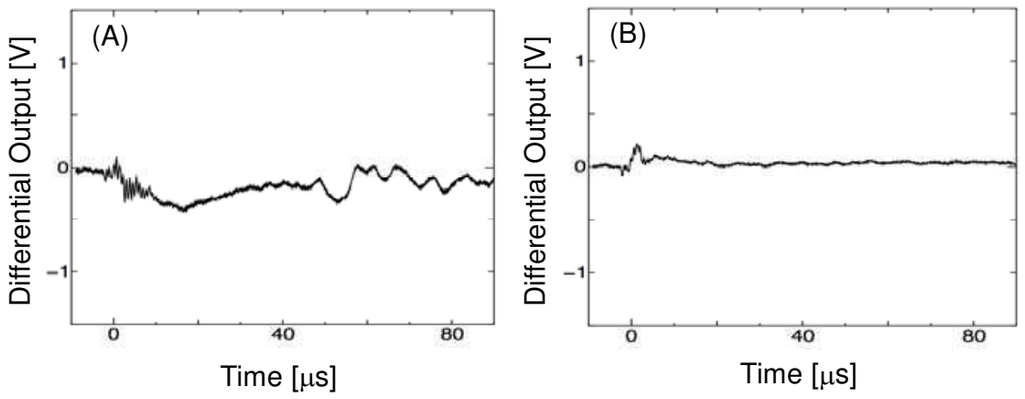

(a)Differential outputs of rotation angles

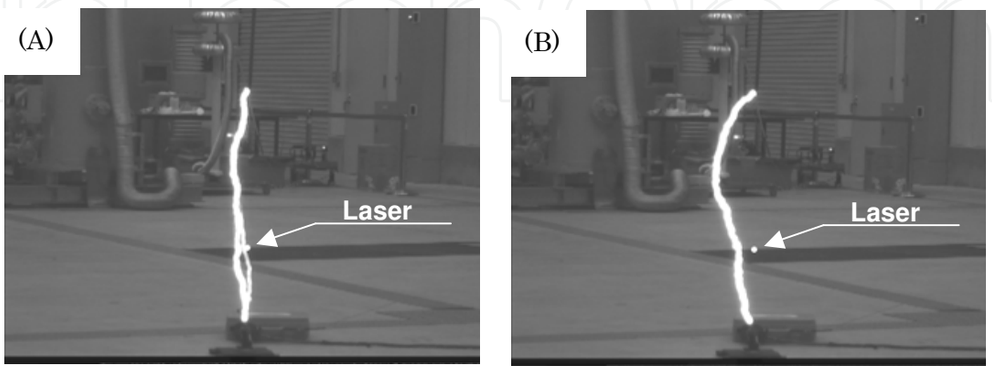

(b)Snapshots of discharge path

Fig. 6-5. Discharge experiment with electromagnetic shield room.

7. High precision polarization lidar

7.1 System setup

The lidar system was developed under the concept of the above lidar design. (Shiina, 2007a & 2008c) A schematic diagram is shown in Fig. 7-1, a photograph is shown in Fig. 7-2, and the specifications are summarized in Table 7-1. The optical circulator and a pair of Axicon prisms were installed into the lidar optics to realize the in-line optics. All optical components were selected to realize the high polarization extinction ratio and the high-power light source.

The laser source is a second harmonic Nd:YAG laser of wavelength 532 nm and pulse energy 200mJ. The polarization plane of the beam is balanced by a half wave plate (HWP) so the intensities of the parallel (*p*-) and orthogonal (*s*-) component beams are equal. The controlled beam passes through the specially designed polarization independent optical circulator. The beam changes its wave shape to the annular by a pair of Axicon prisms to expand its beam size up to the telescope diameter and to prevent the second mirror of the telescope from blocking the beam. All of the optics including the Axicon prisms had small tilts at the flat surface and AR coatings in every surface because the directly reflected light goes back to the detectors. Nevertheless, gated photomultiplier tubes (PMTs) are used for detection. The gate function stops the PMT operation until the outgoing beam exits the lidar optics. This protects the PMTs from reflections of the high power laser pulse from optical components in the in-line optics. The time delay between the beam firing and the start of the gate function is 0.2 μs. In other words, the system can detect the lidar echo signals from the near range of >30 m.

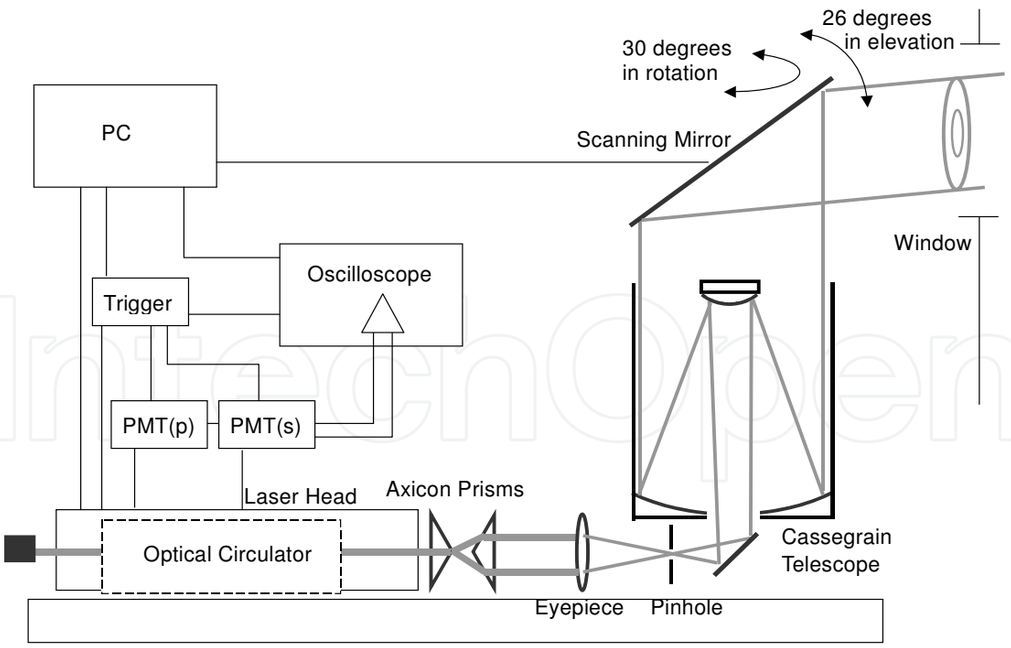

Fig. 7-1. Systematic diagram of high-precision polarization lidar system.

The scanning mirror was installed into the lidar system. The scanning area of the observation was limited to 26 degrees in elevation and 30 degrees in azimuth because of the constraint of the installation site.

To detect the small rotation angle of < 1 degree, the polarization-independent optical circulator for high power green laser was developed, as shown in Fig. 7-3. To avoid damage from the strong incident laser pulse, half wave plates (HWP), Gran laser prisms (GLP), Faraday rotators (FR), and mirrors (M) were chosen based on high threshold for optical tolerance, high transmittance (high reflectance for mirrors), and high extinction ratio for the polarization. The linearly polarized beam is divided equally at GLP1 into orthogonal polarization beams, which go through each path and are joined together at GLP2. The combined beam is transmitted into the Axicon prisms. When the lidar echo re-enters the optics, the parallel (*p*-) polarization echo to the incident beam is detected at GLP3. The echo

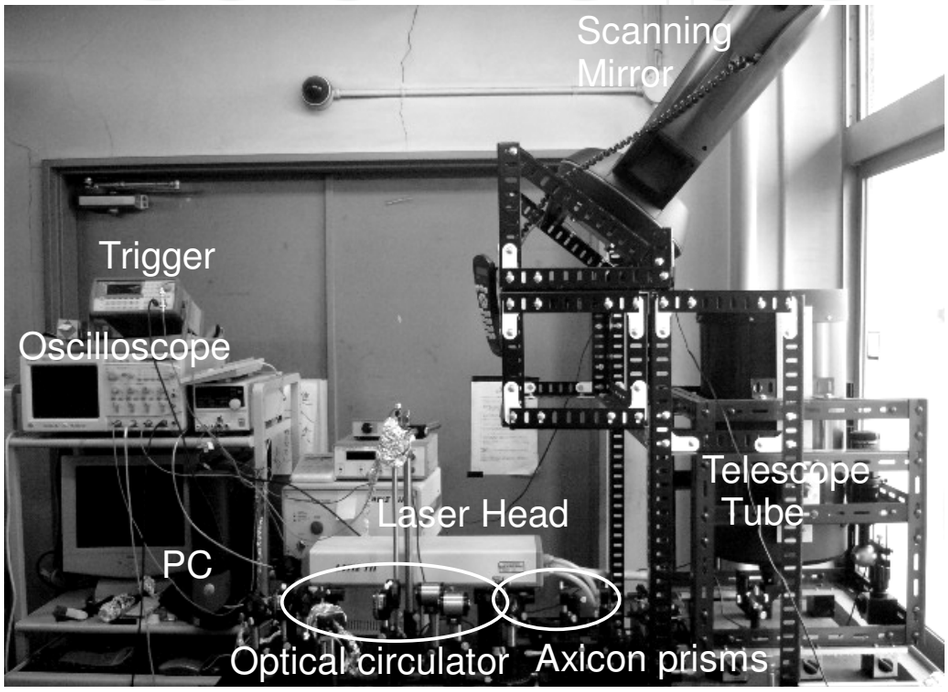

Fig. 7-2. Snapshot of high precision polarization lidar system.

Laser	*Nd:YAG* laser (Lotis TII)	
	Pulse Energy	200 mJ
	Wavelength	532 nm
	Repetition rate	10 Hz
	Beam Diameter	27 cmϕ
Telescope	Shmidt-Cassegrain *(Celestron NextarGPS)*	
	Aperture	28 cmϕ
	Field of View	0.177 mrad
Detector	PMT with gate function (2 ports for p- and s-polarizations) *(Hamamatsu K.K.)*	
	Filter bandwidth	3 nm
Observation	Range	0-20 km(max)

Table. 7-1. Lidar Specifications.

is picked up in the direction perpendicular to the illustration. The orthogonal (*s*-) polarization echo goes back into the circulator and is detected at GLP1. The isolation and the insertion loss of the optical circulator are summarized in Table 7-2. The transmission efficiency of the laser beam was 1.05 dB (79%) on average, which is acceptable considering the transmittances of the optical components. It is also confirmed that the GLP had a sufficiently high extinction ratio of >30 dB for the polarization.

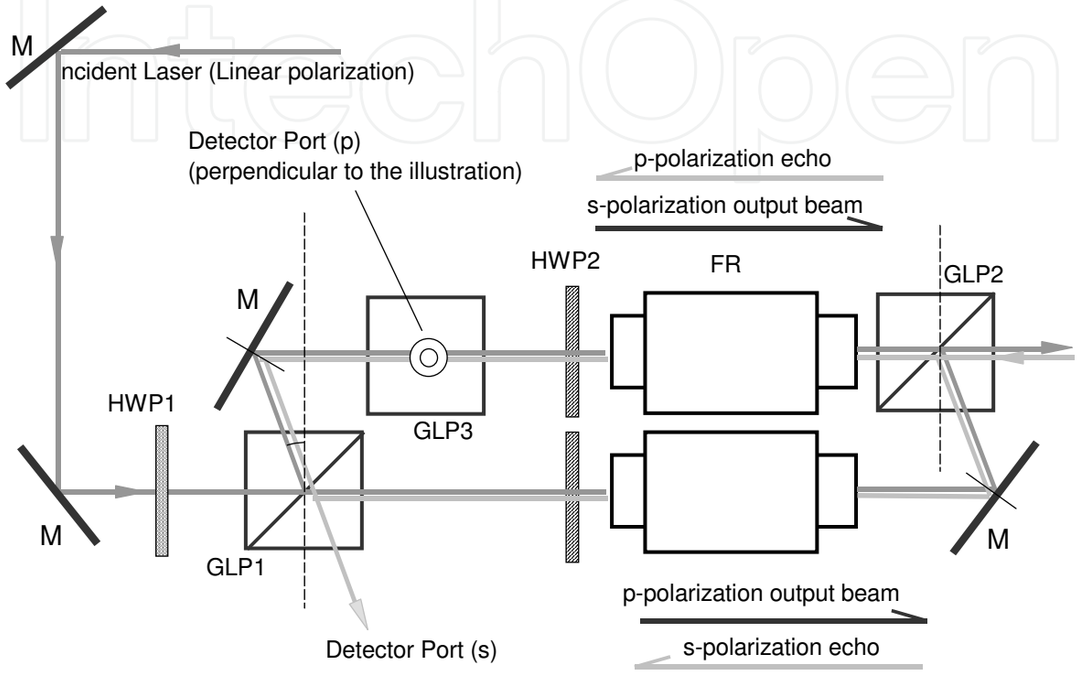

Fig. 7-3. Polarization-independent optical circulator.

Mode	Pol.	Insertion loss [dB]	Isolation	
			p-pol. echo [dB]	*s*-pol. echo [dB]
Transmitter	*p*	1.01	>39	>39
	s	1.08		
Receiver	*p*	1.25	-	>35.9
	s	1.65	>35.4	-

Table 7-2. Performance of polarization independent optical circulator.

7.2 Measurement

Here, echo characteristics of the high precision polarization lidar are explained in perspective of measurement range, intensity balance between p- and s-polarization components, and accuracy. Thanks to the in-line optics, the echo can be detected from near range of 30-50 m. Since the near range echo is large, the receiver's trigger is delayed by the gate function of PMT to restrict the current, especially in the case of far range measurement. If the PMT output current is too large, the balance between p- and s-polarizations is disrupted. In the following figures, the delay was adjusted adequately. Echoes were obtained from 330 m in Fig. 7-4, and from 820m in Figs. 7-5-7-7. We have confirmed that the

delay of more than 3.5-4.0 μs (the lidar echo distance of 500-600 m) is acceptable to obtain the balanced echoes.

At first, the calculated accuracy of rotation angle of the polarization plane was checked by using a hard target. Figure 7-4 shows the p- and s-component echoes from a lightning rod located at a distance of 480 m from the lidar. As this distance is not large enough to eliminate the large echoes, p- and s-polarization echoes were not equal especially in near range of <400m. The echoes were summed over 1024 shots. As the lightning rod is a cylinder, the incident beam is depolarized if it was hit on a decline. Here we evaluated the depolarization as the rotation angle to check the accuracy of the lidar echoes. By using the derivation from Equation (6-1), the rotation angle was calculated as –0.497 degrees. The negative sign indicates the clockwise rotation of polarization plane in Fig. 6-1, that is, s-polarization component was larger than p-component. This result indicates the ability for the detection of the small rotation angle of 1 degree.

Figure 7-5 shows the balance and the accuracy of the echo intensities in the high precision polarization lidar by the atmospheric fluctuations. The figure shows the difference between p- and s-component echoes summed over 4096 shots. The difference at <1 km is large, while that at far distance becomes small, of the order of <100 μV. This difference indicates the accuracy of rotation angle of +/-0.35. That is, the atmospheric fluctuation is restricted enough to identify the rotation due to a lightning discharge. The accuracy, however, is obtained under summation over a large number of shots. The lightning discharge has the duration in the order of a 10-100 μs. See Fig.6-4). Although the cloud-to-cloud discharge continues a few dozens times, the summation should be finished within the period.

The low-altitude cloud observation is shown in Fig. 7-6. The vertical axis is the range-corrected signal ($P_L L^2$) shown in logarithmic scale. The water cloud was detected at 2.34 km ahead. Although p- and s-component echoes from the cloud base were equal intensity, the difference became large at the inside of the cloud. The incident beam penetrated up to 500-600m. The effect of multiple scattering becomes large when the beam penetrates inside cloud. The high precision polarization lidar has the narrow FOV of 0.177 mrad, which successfully eliminated multiple scattering inside the cloud at about 300m. However, the contribution of multiple scattering cannot be ignored for echoes from deeper locations

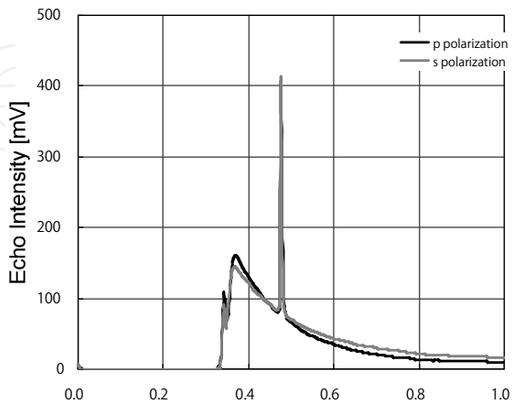

20:00() 24.7.2009, Temp. 25.1 deg, Hum. 62%

Fig. 7-4. Hard target detection.

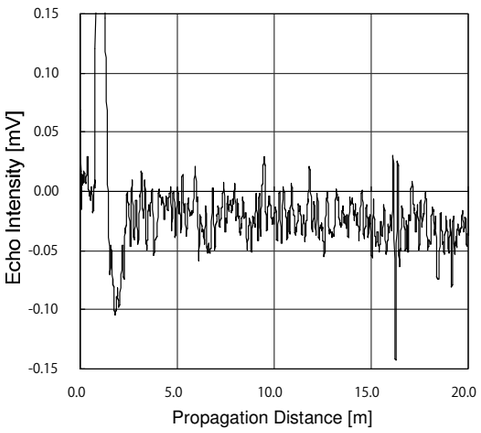

19:49 31.7.2009 Temp. 25.1 deg, Hum. 62%

Fig. 7-5. Accuracy check for long propagation distance.

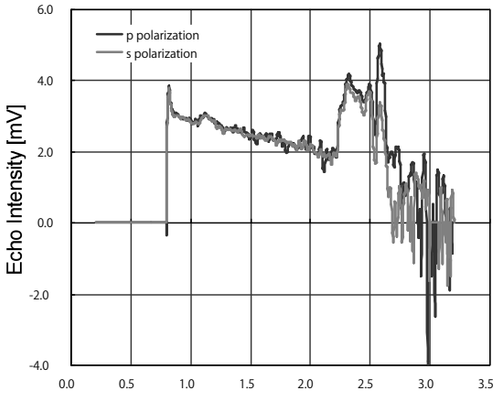

21:06 29.7.2009 Temp. 27.6 deg, Hum. 82%

Fig. 7-6. Cloud observation.

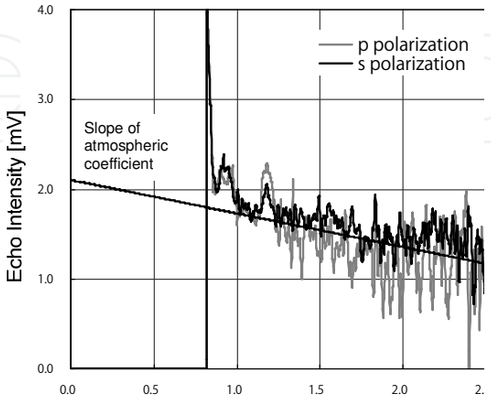

21:00 31.7.2009 Temp. 27.6 deg, Hum. 82%

Fig. 7-7. Estimation of atmospheric coefficient.

inside clouds. The lidar echoes were also examined in the viewpoint of the atmospheric extinction coefficient. The atmospheric extinction coefficient is derived from the slope of the range-corrected signal, shown in Fig. 7-7. The p- and s-component echoes were well balanced. Although the small peak at 1.2km was a thin cloud, there are no influence to the backward echoes. The visibility calculated by the atmospheric coefficient was well coincide with the actual visibility. The near range echo also has the enough accuracy to evaluate the atmospheric characteristics.

8. Summary

Lidars for local weather prediction for prevention of disasters such as heavy rain and lightning strike were developed. As in-line optics were adopted to the in-line MPL and the high precision polarization lidar, the near range measurement could be accomplished with the narrow FOV. Optical circulators were also developed originally not to only separate echoes from the transmitting beam, but also to detect the orthogonal polarization echoes. The polarization extinction ratio between p- and s-polarization echoes was about 20 dB in the in-line MPL. The system can distinguish the ice-crystals from spherical particles stably in long period. The extinction ratio was improved to more than 30dB in the high precision polarization lidar. This improvement realized the measurement of Faraday effect caused by lightning discharge.

The current approach led to application of lidar to detection of hazardous gases. A mini Raman lidar with in-line optics to detect the hydrogen gas leak in near range is currently under development. A mini lidar to monitor the closed space atmosphere such as a factory and an exhibition hall is also under development.

The lidar studies made progress to the another field too. We found that the annular beam used in the in-line lidar optics transforms its intensity distribution into that of the non-diffractive beam through the propagation and that the transformed beam has the tolerant characteristics in the atmospheric fluctuation.(Shiina, 2007b) Now The technique tries to apply to penetrate the longer distance or to monitor the deeper area in the dense scattering media.

The near range detectable in-line lidar is counted on continued outstanding success to the various application by adjusting its size and specifications.

9. Acknowledgement

The author would like to express his thanks to Tetsuo Fukuchi of Central Research Institute of Electrical Power Industry and Kazuo Noguchi of Chiba Institute of Technology for their supports in developing the lidars and discussing the data analyses. These studies were funded by the Grant-in-Aid for Young Scientists (A) and (B), Mitutoyo Association for Science and Technology, and Kansai Research Foundation for technology promotion.

10. Reference

American National Standards Institute, “American national standard for the safe use of lasers”, ANSI Z136.1-1986, pp.1-96, 1986.

C. J. Grund and S. P. Sandberg, “Depolarization and Backscatter Lidar for Unattended Operation”, Advanced in Atmospheric Remote Sensing with Lidar, A. Ansmann, R.

Neuber, P. Rairoux, and U. Wandinger eds.(Springer-Verlag, Berlin, 1996), pp.3-6, 1996

C. Théry, "Evaluation of LPATS data using VHF interferometric observations of lightning flashes during the Eulinox experiment", Atmospheric Research, Vol. 56, Issues 1-4, 397-409, 2001

C. Weitkamp, *Lidar Range-Resolved Optical Remote Sensing of the Atmosphere*, Springer, 2005

D. R. MacGorman, W. L. Taylor, "Positive cloud-to-ground lightning detection by a direction-finder network", Journal of Geophysical Research, Vol. 94, No. D11, 13,313–13,318, 1989

E. Franzblau and C. J. Popp, "Nitrogen oxides produced from lightning", J. Geophys. Res., Vol.94, No.D8, pp.11.089-11.104, 1989

E. Franzblau, "Electrical discharges involving the formation of NO, NO_2, HNO_3, andO_3" , J. Geophys. Res., Vol.96, No.D12, pp.22.337-22.345, 1991

E. J. Welton, J. R. Campbell, J. D. Spinhirne,a nd V. S. Scott, "Global monitoring of clouds and aerosols using a network of micro-pulse lidar systems", in Lidar Remote Sensing for Industry and Environmental Monitoring, U. N. Singh, T. Itabe, N. Sugimoto eds., Proc. SPIE, 4153, pp.151-158, 2001.

G. Indebetouw, "Nondiffracting Optical Fields: Some Remarks on their Analysis and Synthesis", J. Opt. Soc. Am. A, Vol. 6, No. 1, pp.150-152, 1989

G. Scott and N. McArdle, "Efficient Generation of Nearly Diffraction-Free Beams using an Axicon", Opt. Engin., Vol. 31, No. 12, pp.2640-2643, 1992

G. Zaccanti, P. Bruscaglioni, M. Gurioli, and P. Sansoni, "Laboratory simulations of lidar returns from clouds : experimental and numerical results", App. Opt., Vol. 32, No. 9, pp.1590-1597, 1993

H. S. Lee, I. H. Hwang, J. D. Spinhirne, V. Stanley Scott, "Micro Pulse Lidar for Aerosol and Cloud Measurement", Advanced in Atmospheric Remote Sensing with Lidar, A. ansmann, R. Neuber, P. Rairoux, and U. Wandinger eds.(Springer-Verlag, Berlin, 1996), pp.7-10, 1996

I. H. Hwang, M. K. Nam, B. Ranganayakamma, and H. S. Lee, "A Compact Eye-safe Dual Wavelength Lidar and Application in Biological Aerosol Detection", Lidar Remoet Sensing in Atmospheric and Earth Sciences Pert I, L. Bissonnette, G. Roy, and G. Vallee eds.(Defence R&D Canada, 2002), pp. 205-208, 2002

J. D. Spinhirne, "Micro Pulse Lidar", IEEE trans. Geosc. Rem. Sens., Vol. 31, No. 1, pp.48-55, 1993.

J. D. Spinhirne, "Micro Pulse Lidar Systems and Applications", Proceedings of 17th International Laser Radar Conference, pp.162-165, 1994.

J. D. Spinhirne, E. J. Welton, J. R. Campbell, "Measurement of the Vertical Distribution of Aerosol by Globally Distributed MP Lidar Network Sites", IEEE IGARSS 2001Meeting, Sydney, July 2001.

J. Durnin and J. J. Miceli, Jr., "Diffraction-Free Beams", Phys. Rev. Lett., Vol. 58, No. 15, pp.1499-1501, 1987

J. Harms, "Lidar return signals for coaxial and noncoaxial systems with central obstruction", Appl. Opt., Vol. 18, No. 10, pp.1559-1566, 1979

J. S. Ryan, S. R. Pal, and A. I. Carswell, "Laser backscattering from dense water-droplet clouds", J. Opt. Soc. Am., Vol. 69, No. 1, pp.60-67, 1979

J. Stith, J. Dye, B. Ridley, P. Laroche, E. Defer, K. Baumann, G. Hubler, R. Zerr, and M. Venticinque, "NO signature from lightning flashes", J. Geophys. Res., Vol.104, No.D13, pp.16.081-16.089, 1999

K. Kawahata and S. Okajima, "Interferometry and Polarimetry –Principle of Interferometry and Polarimetry-", Japan Society of Plasma Science and Nuclear Fusion Research, Vol.76, No.9, pp.845-847, 2000(written in Japanese)

K. Kono, Y. Mitarai, and T. Minemoto, "New Super-Resolution Optics with Double-Concave-Cone Lens for Optical Disk Memories", J. Opt. Mem. Neural Networks, Vol. 5, No. 4, pp.279-285, 1996

K. Kono, M. Irie, and T. Minemonto, "Generation of Nearly Diffraction-Free Beam Using a New Optical System", Opt. Rev., Vol. 4, No. 3, pp.423-428, 1997

K. Sassen and R. L. Petrilla, "Lidar depolarization from multiple scattering in marine stratus clouds", App. Opt., Vol. 25, No. 9, pp.1450-1458, 1986

K. Sassen, "The polarization lidar technique for cloud research: A review and current assessment", Bulletin American Meteorological Society, Vol.72, No.12, pp.1848-1866, 1991

L. L. Doskolovich, S. N. Khonina, V. V. Kotlyar, I. V. Nikolsky, V. A. Soifer, and G. V. Uspleniev, "Focusators into a Ring", Opt. Quant. Elect., Vol. 25, pp.801-814, 1993

M. Kerscher, W. Krichbaumer, M. Noormohammadian, and U. G. Oppel, "Polarized Multiply Scattered LIDAR Signals", Opt. Rev., Vol. 2, No. 4, pp.304-307, 1995

M. Gai, M. Gurioli, P. Bruscaglioni, A. Ismaelli, and G. Zaccanti, "Laboratory simulations of lidar returns from clouds", App. Opt., Vol. 35, No. 27, pp.5435-5442, 1996

N. Sugimoto, I. Matsui, and Y. Sasano, "Design of lidar transmitter-receiver optics for lower atmospheric observations: geometrical form factor in lidar equation", Jpn. J. Opt., Vol.19, No.10, pp. 687-693, 1990

P. Belanger and M. Rioux, "Ring Pattern of a Lens-Axicon Doublet Illuminated by a Gaussian Beam", Appl. Opt., Vol. 17, No. 7, pp.1080-1086, 1978

P. Bruscaglioni, A. Ismaelli, G. Zaccanti, M. Gai, and M. Gurioli, "Polarization of Lidar Returns from Water Clouds : Calculations and Laboratory Scaled Measurement", Opt. Rev., Vol. 2, No. 4, pp.312-318, 1995

R. Arimoto, C. Saloma, T. Tanaka, and S. Kawata, "Imaging Properties of Axicon in a scanning optical system", Appl. Opt., Vol. 31, No. 31, pp.6653-6657, 1992

R. M. Measures, *Laser Remote Sensing*, John Wiley & Son, New York, 1984.

S. Hayashi, "Numerical Simulation of Electrical Space Charge Density and Lightning by using a 3-Dimensional Cloud-Resolving Model", Scientific Online Letters on the Atmosphere, Vol. 2, p.124-127, 2006

S. R. Pal and A. I. Carswell, "Polarization properties of lidar backscattering from clouds", Appl. Opt., Vol. 12, No. 7, pp.1530-1535, 1973

Society of Atmospheric Electricity of Japan, Atmospheric Electricity, Chapter 2, Corona publishing Tokyo, 2003 (Written in Japanese)

T. Halldorsson and J. Langerholc, "Geometrical form factors for the lidar function", Appl. Opt., Vol. 17, No. 2 pp. 240-244, 1978

T. Hauf, U. Finke, S. Keyn, O. Kreyer, "Comparison of a SAFIR lightning detection network in northern Germany to the operational BLIDS network", Journal of Geophysical Research 112(d18): D18114, 2007

T. Fujii and T. Fukuchi, *Laser Remote Sensing*, Taylor & Francis, 2005

T. Fukuchi, K. Nemoto, K. Matsumoto, and Y. Hosono, “Visualization of High-speed Phenomena using an Acousto-optic Laser Deflector”, IEEJ Transactions on Fundamentals and Materials, Vol.125-A, No.2, pp.113-118, 2005 (written in Japanese)

T. Fukuchi and T. Shiina, “Measurement of rotation of polarization plane of laser radiation propagating though impulse discharge in air”, IEEJ Transactions on Electrical and Electric Engineering, in press.

T. Shiina, E. Minami, M. Ito, and Y. Okamura, "Optical Circulator for In-line Type Compact Lidar", Applied Optics, Vol. 41, No. 19, pp.3900-3905, 2002

T. Shiina, K. Yoshida, M. Ito, and Y. Okamura, “In-line type micro pulse lidar with annular beam -Experiment-”, Applied Optics, Vol.44, No.34, pp.7407-7413, 2005a

T. Shiina, K. Yoshida, M. Ito, and Y. Okamura, “In-line type micro pulse lidar with annular beam -Theoretical Approach-”, Applied Optics, Vol.44, No.34, pp.7467-7473, 2005b

T. Shiina, T. Honda, and T. Fukuchi, "High-precision polarization lidar - lidar in-line optics - ", CLEO Pacific Rim 2007 proceedings, pp.1499-1500, 2007a

T. Shiina, M. Ito, and Y. Okamura, "Long range propagaion characteristics of annular beam", Optics Communications, Vol.279, pp.159-167, 2007b

T. Shiina, T. Honda, and T. Fukuchi, “Evaluation of polarization angle rotation of propagating light in a partially ionized atmosphere under discharge conditions”, Electrical Engineering in Japan, Vol.163, No.4, pp.1-7, 2008a

T. Shiina, T. Honda, and T. Fukuchi, “Optical measurement of high-voltage discharge in air for lidar lightning detection”, APLS The Review of Laser Engineering Supplemental Volume 2008, Vol.36, pp.1279-1282, 2008b

T. Shiina, Masakazu Miyamoto, Dai Umaki, Kazuo Noguchi and Tetsuo Fukuchi, "Fundamental Measurement by In-line typed high-precision polarization lidar", SPIE Asia-Pacific Remote Sensing 2008 proceedings, Vol.7153, pp.71530B-1 - 71530B-8, 2008c

T. Shiina, T. Honda, and T. Fukuchi, “Measurement of polarization rotation of propagating light in a partially ionized atmosphere under discharge conditions”, Electrical Engineering in Japan, in press.

V. Soifer, V. Kotlyar, and L. Doskolovich, *Iterative Methods for Diffractive Optical Elements Computation*, Tatlor & Francis, 1997

Y. Matsudo, T. Suzuki, M. Hayakawa, K. Yamashita, Y. Ando, K. Michimoto, V. Korepanov, “Characteristics of Japanese winter sprites and their parent lightning as estimated by VHF lightning and ELF transients”, Journal of atmospheric and solar-terrestrial physics, vol.69, no.12, 1431-1446, 2007

Advances in Solid State Lasers Development and Applications

Edited by Mikhail Grishin

ISBN 978-953-7619-80-0
Hard cover, 630 pages
Publisher InTech
Published online 01, February, 2010
Published in print edition February, 2010

Invention of the solid-state laser has initiated the beginning of the laser era. Performance of solid-state lasers improved amazingly during five decades. Nowadays, solid-state lasers remain one of the most rapidly developing branches of laser science and become an increasingly important tool for modern technology. This book represents a selection of chapters exhibiting various investigation directions in the field of solid-state lasers and the cutting edge of related applications. The materials are contributed by leading researchers and each chapter represents a comprehensive study reflecting advances in modern laser physics. Considered topics are intended to meet the needs of both specialists in laser system design and those who use laser techniques in fundamental science and applied research. This book is the result of efforts of experts from different countries. I would like to acknowledge the authors for their contribution to the book. I also wish to acknowledge Vedran Kordic for indispensable technical assistance in the book preparation and publishing.

INTECH
open science | open minds

InTech Europe
University Campus STeP Ri
Slavka Krautzeka 83/A
51000 Rijeka, Croatia
Phone: +385 (51) 770 447
Fax: +385 (51) 686 166
www.intechopen.com

InTech China
Unit 405, Office Block, Hotel Equatorial Shanghai
No.65, Yan An Road (West), Shanghai, 200040, China
中国上海市延安西路65号上海国际贵都大饭店办公楼405单元
Phone: +86-21-62489820
Fax: +86-21-62489821

IntechOpen